KSME

Springer

Journal of Mechanical Science and Technology 34 (5) 2020

Original Article
DOI 10.1007/s12206-020-0429-4

Keywords:
· Viscoplasticity
· Moisture and heat transport
· Paper curl
· Porous medium

Correspondence to:
Seungjun Lee
sjunlee@dgu.ac.kr

Citation:
Yoon, G. H., Yoo, B., Kim, W. K., Woo, J., Kim, T., Lee, S. (2020). Multiphysics simulation of paper curl due to moisture transport. Journal of Mechanical Science and Technology 34 (5) (2020) 2075~2083. http://doi.org/10.1007/s12206-020-0429-4

Received February 21st, 2019
Revised January 14th, 2020
Accepted March 3rd, 2020

† Recommended by Editor Seungjae Min



# Multiphysics simulation of paper curl due to moisture transport

**Gil Ho Yoon[1], Byoungho Yoo[2], Woon Kyung Kim[2], Junseong Woo[2], Taehan Kim[2] and Seungjun Lee[3]**

[1]School of Mechanical Engineering, Hanyang University, Seoul 04763, Korea, [2]HP Printing Korea Co., Ltd, Seongnam 13529, Korea, [3]Department of Mechanical, Robotics, and Energy Engineering, Dongguk University, Seoul 04620, Korea

**Abstract** The moisture transport at the fuser nip of printers is postulated to be the main reason for paper curls. However, the fundamental mechanisms of paper curling remain unclear. Observing the moisture transport inside a sheet of paper through experiments is difficult because moisture transport rapidly occurs in a micro-scale thickness. Therefore, developing a theoretical model is crucial to understand the mechanisms of paper curling and to control the curls. In this study, we proposed a multiphysics model that includes the moisture and heat transport and mechanical deformation. The elasticity, plasticity, viscosity, and expansion caused by moisture were considered in the mechanical model to describe the complex material characteristics of paper. The curvature of curls was calculated using an effective two-spring model. The mechanisms of curling in printers and the direction of curls were understood through finite element simulations. The proposed model can qualitatively predict the paper curls observed in experiments. The temperature- and moisture-dependent material properties of paper will be studied in the future to improve the proposed model.

## 1. Introduction

Paper curl is undesirable because it lowers printing quality and causes paper jams in machines. The curling of paper after printing is mainly because of the moisture transport inside its fabric network, as shown in Fig. 1(a) [1-7]. The excessive curling of paper is challenging, as shown in Fig. 1(b), particularly in tropical regions, where considerable moisture is absorbed by the paper because of hot and humid environments. Predicting and controlling paper curl is important in the printing industry. However, measuring the moisture transport through experiments is difficult because it rapidly occurs and in micro-sized pores. Therefore, a theoretical model should be developed for the moisture transport inside the paper.

The causes of paper curl in printing machines can be categorized into three groups, namely, the fuser nip curl caused by high temperature and pressure at the fusing nip, the path curl caused by severely curved path, and the contraction curl caused by the solidification of toner or ink. In this study, we focus on the fuser nip curl, which is the major type of curling. A multiphysics model is developed, and the evolution of moisture and temperature inside the paper is calculated to predict the paper curls that pass through the fuser nip. The obtained moisture content is linked with mechanical deformation to calculate the level of curling. The calculated curvature of paper is compared with the experimental measurements.

Ink or toner is spread over the paper sheet inside the fuser of copy machines or printers. The paper surface is exposed to high temperature using a heat roller (HR) for consolidating the ink or toner by drying the contained moisture. This sudden heat exposure causes the moisture to be transported throughout the thickness of the paper. The moisture transport results in a gradient of moisture content in the paper, leading to the swelling or shrinking of the its surfaces. Curls can be generated toward the hot surface or toward the cool surface, as shown in Figs. 1(c) and (d).

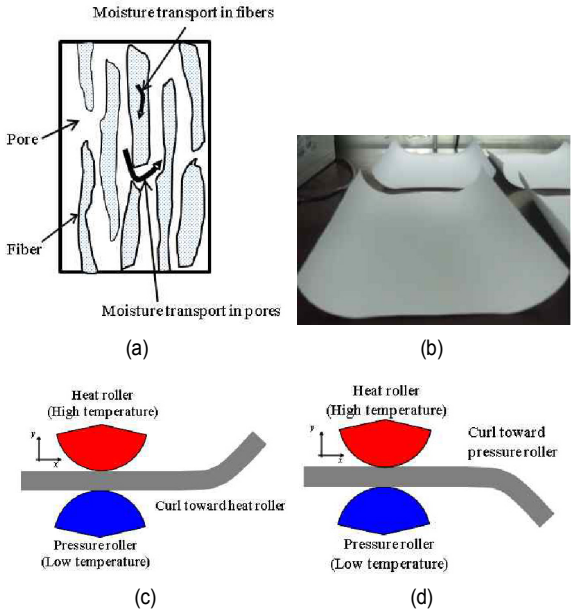


Fig. 1. Paper curls after printing: (a) Moisture transport inside the porous fabric network of paper; (b) example of paper curl after printing, and schematic of paper curl; (c) toward the HR; (d) toward the pressure roller (PR).

Significant efforts have been exerted on the study of moisture transport inside cellulose-based materials in the relevant engineering fields [5]. Paper has been modeled as an elasto-plastic material to simulate cockling, curling, and fluting, and computational simulations have revealed that the moisture gradient is an important factor for the cockling phenomenon [8]. A theoretical model was developed to predict the distribution of moisture content throughout the thickness, and the deformation of papers and cardboards subjected to relative humidity change was studied [9]. A coupled numerical model was developed for the hydraulic fracture propagation in porous media using an extended finite element method [10]. A time marching technique was developed to analyze hyperbolic bioheat transfer problems [11]. The diffusion-induced dimensional change called hydroexpansion was simulated in various studies by controlling the diffusion distance and diffusion coefficient [12]. A multiphase model was developed to study the moisture transport and evaporation inside fibrous porous materials [6, 13]. A transient multiphysics mathematical model of coupled heat and moisture transfer through fibrous insulation was formulated, and the influencing factors on heat flux were identified [14]. A theoretical model for water vapor transport in cellulose-based materials was developed, and the water transmission rates were compared with the experimental measurements [15]. Theoretical models were introduced to describe the moisture diffusion in paper at different humidity [1-5]. Moisture transport models were proposed to understand the water diffusion in a stack of paper sheets under steady-state and transient conditions [16, 17]. The mechanical forming properties of fabric were obtained through direct measurement and inverse modeling [18]. Macroscale and network models were utilized to explain the out-of-plane deformation [19].

Although the coupling of moisture transport and temperature change has been addressed by few studies, it has rarely been used to analyze the coupling of moisture transport, temperature, and mechanical deformation. In terms of mechanics, the curled paper will flatten when the paper sheet is assumed to be an elastic material. The paper should be treated as a viscoplastic material to simulate permanent deformation. Simulating the residual deformation caused by the moisture transport inside the fibrous paper is difficult.

In this study, we present a multiphysics simulation for the moisture transport inside the paper caused by temperature changes and mechanical deformation caused by moisture changes. All equations are numerically solved using the finite element method. Inspired by bimetal bending, the mechanical deflection is described using a two-spring model, thereby allowing the effective calculation of paper curls, including the complex mechanical properties of elasticity, plasticity, and viscosity of paper. In the simulation, the paper passes through a fuser nip between a hot roller and a cool roller and is then exposed to the environment. To simulate this process, four equations, namely, the moisture transport in the pores, moisture transport in the fibers, temperature change in the paper, and mechanical deformation, are coupled in the calculation. Experiments are conducted under varying temperatures of the rollers to verify the propose model. The simulations performed under similar conditions exhibit a similar trend in terms of the amount of curls. The convection effect is simulated to understand the role of fan on the paper surface.

## 2. Mathematical model for moisture, temperature, and mechanical deformation

### 2.1 Moisture transport

The partial differential equations about moisture transport inside the paper have been derived in the previous work [1]. We summarize these equations in this section. Consider a representative element volume inside the paper consisting of two domains of cellulose fibers "f" (blue) and pores "p" (white), as shown in Fig. 1(a). The time-dependent moisture concentration at each domain can be expressed as

$$(1-\eta)\frac{\partial c_f}{\partial t} = (1-\eta)\nabla\cdot(D_f\nabla c_f) + S\,, \tag{1}$$

$$\eta\frac{\partial c_p}{\partial t} = \eta\nabla\cdot(D_p\nabla c_p) - S\,, \tag{2}$$

where $\eta$, $c_f$, $c_p$, $D_f$, $D_p$, and $t$ represent the volume ratio of the pores [-], the moisture concentration in the fibers [kgm$^{-3}$], the moisture concentration in the pores [kgm$^{-3}$], the diffusivity of moisture in the fibers [m$^2$s$^{-1}$], the diffusivity of moisture in the pores [m$^2$s$^{-1}$], and time [s], respectively. $S$ represents the exchange of moisture between the fibers and pores and can be described on the basis of a linear relation of the difference between the equilibrium and current concentrations:

$$S = k(c_f^{eq} - c_f), \tag{3}$$

where $k$ [$s^{-1}$] and $c_f^{eq}$ [$kgm^{-3}$] represent the mass transport coefficient and the moisture concentration in equilibrium, respectively. $c_f^{eq}$ can be determined by measuring the moisture isotherm sorption and can be expressed as

$$c_f^{eq} = \frac{\rho M_0 CKH}{(1-KH)(1-KH+CKH)}, \tag{4}$$

where $\rho$ [$kgm^{-3}$] and $H$ are the density of paper and relative humidity, respectively, and $M_0$, $C$, and $K$ are the Guggernheim-Andersen-de Boer (GAB) parameters [20, 21]. The relative humidity can be expressed as $H = c_p / c^*_p$, where $c^*_p$ is the saturated moisture content in air, which is a function of temperature.

## 2.2 Heat transport

Time-dependent temperature $T$ [K] is described using the heat equation:

$$c\rho\frac{\partial T}{\partial t} = \nabla\cdot(\lambda\nabla T) + (1-\eta)h\frac{\partial c_f}{\partial t}, \tag{5}$$

where $c$ [$Jkg^{-1}K^{-1}$], $\lambda$ [$Jm^{-1}K^{-1}s^{-1}$], and $h$ [$Jkg^{-1}$] represent the specific heat of paper, the thermal conductivity of paper, and the heat of moisture sorption, respectively. The last term is associated with the heat generated by the adsorption/desorption of moisture.

## 2.3 Mechanical deformation

From a mechanical point of view, fibrous papers exhibit a viscoplastic behavior. Choosing a mathematical model that accurately describes the paper curl caused by the change in moisture content is difficult. In this study, the mechanical model is generated by summing the related terms of elasticity, plasticity, viscosity, and moisture expansion. The plasticity is expressed using the Ramberg-Osgood model [22]:

$$\varepsilon = \frac{\sigma}{E} + \alpha\frac{\sigma}{E}\left(\frac{\sigma}{\sigma_y}\right)^{n-1} = \frac{\sigma}{E} + \alpha\frac{\sigma^n}{E}\left(\frac{1}{\sigma_y}\right)^{n-1}, \tag{6}$$

where $\sigma$, $\varepsilon$, $E$, $n$, $\sigma_y$, and $\alpha$ represent the stress, strain, Young's modulus, hardening constant, yield strength, and plastic constant, respectively. To consider the effect of viscosity, a viscosity term is added in the time derivative of Eq. (6):

$$\frac{d\varepsilon}{dt} = \frac{1}{E}\frac{d\sigma}{dt} + \alpha\frac{n}{E}\left(\frac{\sigma}{\sigma_y}\right)^{n-1}\frac{d\sigma}{dt} + \frac{\sigma}{\mu}, \tag{7}$$

where $\mu$ is the viscosity of paper. After the term for the expansion caused by moisture is added, the loading and unloading cases are separately expressed as follows:

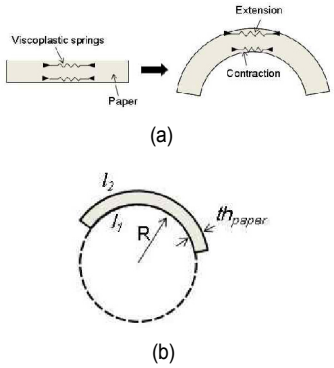


Fig. 2. Two-spring model for the calculation of paper curl: (a) Viscoplastic spring model; (b) curl calculation.

Loading:

$$\frac{d\varepsilon}{dt} = \frac{1}{E}\frac{d\sigma}{dt} + \alpha\frac{n}{E}\left(\frac{\sigma}{\sigma_y}\right)^{n-1}\frac{d\sigma}{dt} + \frac{\sigma}{\mu} + \alpha_W\frac{dc_f}{dt}, \tag{8}$$

Unloading:

$$\frac{d\varepsilon}{dt} = \frac{1}{E}\frac{d\sigma}{dt} + \alpha\frac{n}{E}\left(\frac{\sigma-\sigma_{UL}}{2\sigma_y}\right)^{n-1}\frac{d\sigma}{dt} + \frac{\sigma}{\mu} + \alpha_W\frac{dc_f}{dt}, \tag{9}$$

where $\alpha_W$ represents the moisture expansion coefficient. The stress value when the unloading starts is denoted by $\sigma_{UL}$. $\alpha_W$ typically depends on the paper direction because of the orientation of fibers. The expansion coefficient in the cross direction is four times larger than that in the machine direction.

The material properties should be measured with respect to temperature and moisture. In this study, the Young's modulus and yield stress are modeled to be dependent on moisture and temperature. The dependencies of other material properties on the two factors are ignored in the present study.

## 2.4 Curl calculation

The finite element method is used to numerically solve the coupled equations. Although a 3D model can be used for the simulation using state-of-the art commercial software, many issues, including heavy computation time, mechanical model implementation, and multiscale contacts occur. We adopt the following approach to effectively estimate the amount of curls. The moisture transport is computed in the thickness direction, and the mechanical deformation is calculated in the in-plane direction. To calculate the amount of curling, two mechanical springs are placed at the top and bottom surfaces of the paper, as shown in Fig. 2. The calculated moisture contents in the fiber at the top and bottom surfaces are inserted in the mechanical model to calculate the expansion/shrinkage caused by the change in moisture contents. From the strain of the two springs, the paper curl is calculated using the following equations:

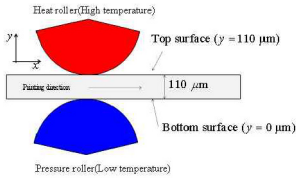


Fig. 3. Diagram of paper moving through the fusing nip.

$$l_1 = R\theta \,, \tag{10a}$$

$$l_2 = (R + th_{paper})\theta \,, \tag{10b}$$

where $l_1$, $l_2$, $R$, $th_{paper}$, and $\theta$ represent the spring length at the bottom surface, spring length at the top surface, curl radius, paper thickness, and bending angle, respectively. Removing the bending angle from Eqs. (10a) and (10b) yields the paper curvature:

$$Curvature: \frac{1}{R} = \frac{(l_2 - l_1)}{l_1 th_{paper}} \,. \tag{11}$$

## 3. Numerical simulations

### 3.1 Paper simulation model

Eqs. (1)-(5), which are related to moisture and heat transport, are numerically solved using the COMSOL Multiphysics® software. The moisture contents inside the paper sheet are stored at every time step, which is fixed at 0.005 s. The stored moisture data are used as input for the MATLAB code to calculate the stress and strain of the paper sheet using Eqs. (8) and (9). Using the calculated strain at the top and bottom surfaces of the paper sheet, the curvature of paper curls is calculated using Eq. (11). The simulation takes approximately 5 min using a typical Windows computer.

Fig. 3 show the schematic of a paper sheet passing through a fusing nip in a laser printer. Inside the fusing nip, the paper is pressed between the PR and HR, in which their temperature is more than 100 ˚C. The temperature of the PR is lower than that of the HR because a heater is only installed on one side of the HR.

As previously mentioned, a 1D multiphysics model is used to calculate the moisture content in the pores and fibers of a paper sheet along the thickness direction. The paper thickness is assumed to be 110 μm. Assuming that the diffusion through the fibers is relatively small compared with the diffusion through the pores, the diffusion terms in the fiber is ignored.

The paper is assumed to be inside and outside the fuser nip at $0 < t < t_1$ and $t_1 < t < t_2$, respectively. Given that the moisture is assumed to transport only through the pores, the moisture fluxes of fiber $c_f$ at the top and bottom surfaces are set to zero. For the moisture concentration of pore $c_p$, the fluxes are set to zero inside the fuser nip and nonzero outside the fuser nip, thereby allowing moisture exchanges with the environment. The boundary conditions for variables $c_p$ and $c_f$ are expressed as follows:

Bottom surface ($y$ = 0):

$$D\frac{\partial c_p}{\partial y} = \begin{cases} 0 & \text{for } 0 < t < t_1 \\ K_m(c_p - c_p^{env}) & \text{for } t_1 < t < t_2 \end{cases} \,, \tag{12a}$$

Upper surface ($y$ = 110 μm):

$$D\frac{\partial c_p}{\partial y} = \begin{cases} 0 & \text{for } 0 < t < t_1 \\ K_m(c_p^{env} - c_p) & \text{for } t_1 < t < t_2 \end{cases} \,, \tag{12b}$$

Bottom and upper surfaces ($y$ = 0 and 110 μm):

$$\frac{\partial c_f}{\partial y} = 0 \,, \tag{13}$$

where $K_m$ is the convective mass transfer coefficient on the paper surfaces, and $c_p^{env}$ is the moisture concentration in the environment.

For the temperature, the top surface of the paper contacts with the HR, and the bottom surface contacts with the PR when the paper is inside the nip. The two surfaces are exposed to the environmental temperature when the paper is out of the nip. The boundary conditions for the temperature are expressed as follows:

Bottom surface ($y$ = 0):

$$\lambda\frac{\partial T}{\partial y} = \begin{cases} K_h^{roller}(T - T^{pr}) & \text{for } 0 < t < t_1 \\ K_h^{air}(T - T^{env}) & \text{for } t_1 < t < t_2 \end{cases} \,, \tag{14a}$$

Upper surface ($y$ = 110 μm):

$$\lambda\frac{\partial T}{\partial y} = \begin{cases} K_h^{roller}(T^{hb} - T) & \text{for } 0 < t < t_1 \\ K_h^{air}(T^{env} - T) & \text{for } t_1 < t < t_2 \end{cases} \,, \tag{14b}$$

where $K_h^{roller}$ and $K_h^{air}$ denote the thermal conductance between the roller and the paper and the heat transfer coefficient between the air and the paper, respectively. $T^{pr}$, $T^{hr}$, and $T^{env}$ denote the temperature of the PR, HR, and room, respectively.

The mechanical boundary condition is represented in accordance with time and location. When the paper is inside the fuser nip, no deformation is allowed because the paper is constrained by two rollers. Otherwise, the stress is relaxed, and deformation is allowed. The mechanical boundary conditions are set as follows:

Bottom and upper surface ($y$ = 0, $y$ = 110 μm):

$$\begin{aligned} &\varepsilon = 0 \ (\sigma \neq 0) \text{ for } 0 < t < t_1 \\ &\sigma = 0 \ (\varepsilon \neq 0) \text{ for } t_1 < t < t_2 \end{aligned} \,. \tag{15}$$

Although the paper can deform because of the roller shape inside the nip, the effect of pressure from the rollers is ignored in this study.

The multiphysics simulation results strongly depend on the material parameters in the coupled equations and the bound-

Table 1. Parameters used in the heat and moisture model [13].

| | | |
|---|---|---|
| $\eta$ | Porosity | 0.47 |
| $k$ | Internal mass transfer coefficient ($s^{-1}$) | 3.5 |
| $D$ | Effective diffusivity of water vapor in pores ($m^2s^{-1}$) | $3\times10^{-6}$ |
| $c$ | Specific heat capacity of paper ($Jkg^{-1}K^{-1}$) | 1200 |
| $\rho$ | Density of paper ($kgm^{-3}$) | 818 |
| $\rho_f$ | Density of fiber ($kgm^{-3}$) | 1500 |
| $\lambda$ | Thermal conductivity of paper ($Wm^{-1}K^{-1}$) | 0.51 |
| $h$ | Adsorption enthalpy of water on fibers ($Jkg^{-1}$) | $2.5\times10^6$ |
| $K_m$ | Convective mass transfer coefficient between paper and air ($ms^{-1}$) | 0.011 |
| $K_h^{roller}$ | Thermal convection between paper and metal ($Wm^{-2}K^{-1}$) | 1180 |
| $K_h^{air}$ | Thermal convection between paper and air ($Wm^{-2}K^{-1}$) | 11.48 |
| $C$ | GAB parameter | 39.09 |
| $M_0$ | GAB parameter | 0.0329 |
| $K$ | GAB parameter | 0.865 |
| $T^{env}$ | Environment temperature (K) | 305 |
| $c_p^{env}$ | Relative humidity | 0.8 |

Table 2. Parameters used in the mechanical model.

| | | |
|---|---|---|
| $E$ | Young's modulus (GPa) | 2.5773 |
| $n$ | Parameter of Ramberg-Osgood model | 4.5 |
| $\alpha$ | Parameter of Ramberg-Osgood model | 0.429 |
| $\sigma_y$ | Parameter of Ramberg-Osgood model (Pa) | $25\times10^6$ |
| $\alpha_W$ | Moisture expansion coefficient | 0.0015 |
| $\mu$ | Viscosity ($kgm^{-1}s^{-1}$) | 27248511 |

ary conditions. The material properties of papers are different because of the randomness of fibers. Determining the exact material properties of paper is an important research area. The material properties in Refs. [4, 23] are utilized for the properties of moisture transport equations and material properties in mechanical equations. The parameters used in the simulation are summarized in Tables 1 and 2, and these values are used unless stated.

## 3.2 Curl simulation 1

The temperatures of the HR and PR are set to 170 ˚C and 100 ˚C, respectively. The environmental temperature is set to 30 ˚C, and the relative humidity is set to 85 %. The paper is assumed to be in equilibrium before printing. The initial moisture concentration in the fiber using Eq. (4) is 12.3 %. The GAB parameters are assumed to be constant, where $M_0$ = 0.0329, $K$ = 0.865, and $C$ = 39.09 [13].

The moisture distributions in the pore and fiber are plotted in Figs. 4(a) and (b), respectively. The moisture in the fiber is equally distributed initially. However, the moisture in the fiber moves toward the center of the paper until $t$ = 0.025 s because

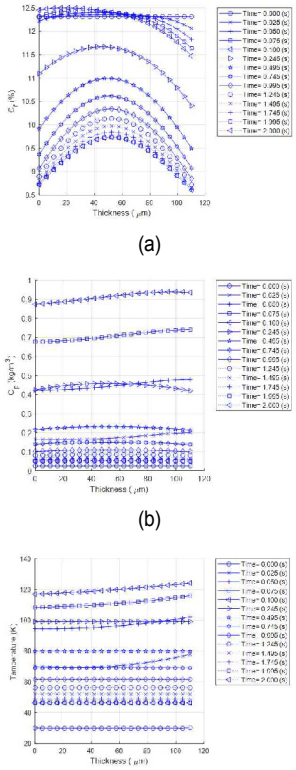

(a)

(b)

(c)

Fig. 4. Moisture and temperature evolutions inside the paper sheet (paper thickness of 110 $\mu m$): (a) Moisture contents in the fiber; (b) moisture contents in the pore; (c) temperature inside the paper.

of the sudden exposure to a high temperature (i.e., 100 ˚C at the bottom surface and 170 ˚C at the top surface). Then, the moisture at the low-temperature side moves toward the high-temperature side when the paper is inside the nip (i.e., until $t$ = 0.1 s). After the paper escapes the nip, the moisture in the fiber rapidly decreases because the moisture evaporates from the bottom and top sides. The moisture of the pore is uniformly distributed initially and gradually increases inside the nip because of the moisture evaporation from the fiber. After the paper is out of the nip, the moisture decreases because it escapes from the two surfaces into the air. The temperature distributions are plotted in Fig. 4(c). The temperature rapidly approaches near the temperature of the HR and PR because of the ramped change in the temperature inside the nip.

After the moisture distributions are calculated, the curl evolution of the paper is computed using the mechanical model, and the result is shown in Fig. 5. The red curve represents the calculated result on the high-temperature side of the HR, and the blue curve represents the result on the low-temperature side of the PR. Fig. 5(a) shows the evolution of moisture content in the fiber at the top and bottom sides. Inside the nip ($t$ = 0.1 s), the moisture in the fiber moves from the high-temperature side to the low-temperature side. After the paper is out of the nip, the moisture on two sides decrease because they escape into the air. Fig. 5(b) shows the stress evolution of the two surfaces.

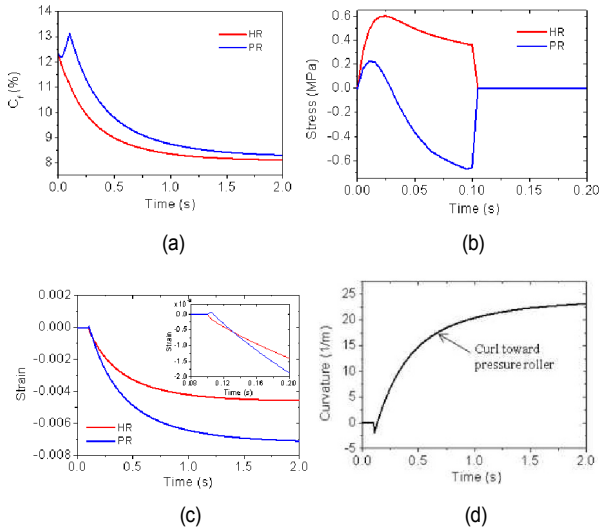


Fig. 5. (a) Evolution of moisture content at the high-temperature (HR) and low-temperature sides (PR); (b) stress evolution; (c) strain evolution (inset figure is a zoomed view around $t$ = 0.1); (d) curvature evolution.

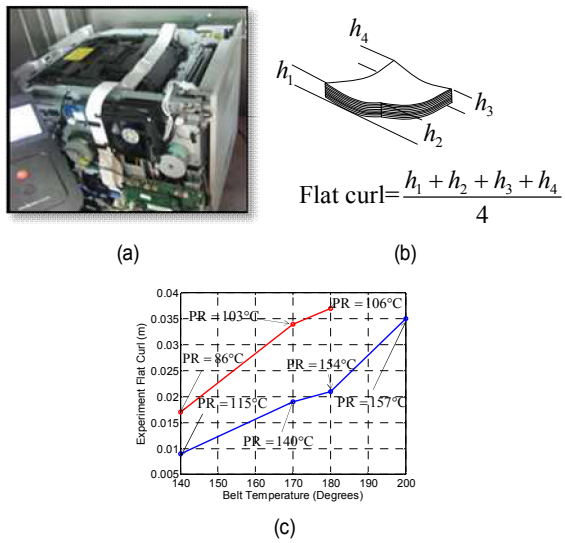


Fig. 6. (a) Printer used in the experiment (paper: Milk 75 g); (b) flat curl computing method; (c) flat curl values measured after 3 min under different operating conditions.

The stress at the low-temperature side is compression because the expansion caused by the increase in moisture content is prevented by the rollers. Similarly, the high-temperature side is under tension because the shrinkage caused by the decrease in moisture content is prevented. After the nip ($t$ > 0.1 s), the stresses are released. Fig. 5(c) shows the strain evolution. The strain is zero when the paper is inside the nip because of the constrained conditions. After the nip, the two ends show a negative strain (compression) because the moisture escapes. However, the amount of contraction is different. The low-temperature side shrinks more than the high-temperature side because of the higher moisture content on the former than on the latter before the escape. Therefore, more moisture escape from the low-temperature side than from the high-temperature side. Thus, the paper is bent toward the low-temperature side. The expected curl direction matches with the result n Fig. 1(b). The zoomed view of the strain variation when the paper is out of the nip is shown in the inset of Fig. 5(c). The strain curves cross each other, showing that the paper is immediately curled toward the high-temperature side after it is out of the nip. This curl generated as the stress developed inside the nip is released, the high-temperature side in tension elongates, and the low-temperature side in compression contracts when the constraints are removed. However, the curl toward the high-temperature side rapidly occurs, and the amount of curl is small. The evolution of paper curvature is shown in Fig. 5(d). The negative values indicate the curls toward the high-temperature side, and the positive values indicate the curls toward the low-temperature side. Inside the nip, no curl is generated because of the constrained conditions. The small curl toward the high-temperature side is generated for a short time when the paper is immediately out of the nip. Then, the curl toward the low-temperature side gradually increases, and its curvature converges to 23 $m^{-1}$.

The simulation results show that the printing paper curls toward the low-temperature side. The curl will be generated toward the high-temperature side when no constraints are applied inside the nip because the moisture transport is from the high-temperature side to the low-temperature side. The paper will then flatten when the moisture escapes from the surfaces. However, the paper does not immediately respond during moisture transport because of the constraints of the rollers. More moisture escape from the low-temperature side, leading to many contractions and curling toward the low-temperature side. Thus, the fuser nip curl depends on the difference in moisture content. Decreasing the temperature difference between the HR and PR will reduce the nip curl because the moisture transport is caused by temperature difference.

### 3.3 Curl simulation 2

For the second example, the simulation results and the measured curls in the experiments performed by HP printing company are compared at various temperatures. The printer used in the experiment is shown in Fig. 6(a). In the experiments, the curl magnitudes are measured using the flat curl method shown in Fig. 6(b). The printed paper is placed on the floor, and the height of the corners of the curled paper is measured and averaged. The experiment is conducted at high temperature of 30 °C and high humidity of 85 %. The paper is placed for one day under the experimental condition to achieve its equilibrium state. All experiments and measurements are conducted in the chamber where the temperature and humidity can be controlled. The environmental condition significantly affects the amount of curls. The curls become severe with the increase in temperature and humidity. The simulations are performed under the same experimental condition. The curls of

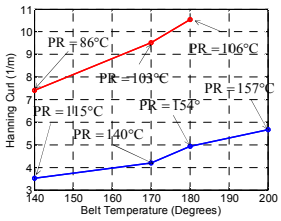


Fig. 7. Calculated curls from the simulations (hanging curl values).

10 paper sheets are averaged. The curls are evaluated by measuring the height of the cured edge of the printed paper sheets after the paper is placed on the flat table (flat curl method). The calculated curls from the simulation can be different from the measured values because the curls measured using the flat curl method are affected by gravity. The experiment results in Fig. 6(c) show that the curls significantly increase with the increase in belt (HR) temperature.

At the same belt temperature, the curl increases with the increase in the temperature difference between the HR and PR.

The paper curls are calculated using the developed simulation code under the same temperature in the experiment. The calculated results are shown in Fig. 7. The calculated curls can be referred to as the hanging curls, which are unaffected by gravity. The overall tendency is extremely similar to that of the experimental result in Fig. 6(c). However, the quantitative comparison is limited because the material properties and the curl measuring method are different. The simulation and experimental results indicate that the HR temperature and the temperature difference between the HR and PR affect the paper curl because they influence the moisture difference between the top and the bottom surfaces of the paper.

In the experiment, the curl at 200 °C of the HR and 243 °C of the PR is similar to the curl at 180 °C of the HR and 254 °C of the PR considering the gravity. However, this trend is not shown in the simulation results. This discrepancy is assumed to arise from the temperature/moisture-dependent material properties of real paper. The material properties of Young's modulus, yield stress, viscosity, and power *n* in Eq. (7) may change in accordance with the temperature and moisture content, which are ignored in the simulations. The paper properties that depend on temperature and moisture will be studied in future work.

## 3.4 Curl simulation 3

In this experiment, the effect of a fan on paper curl is investigated. The temperature and the moisture convection can be controlled by controlling the flow rate with the installation of a fan because the moisture evaporation through the surfaces is a key factor for the curl. The fan can be placed at the front side or the rear side. After passing between the two rollers, most of the moisture transported toward the low-temperature surface is evaporated, resulting in the inverse curl. Therefore, the curl may become significant by installing a fan at the rear side of the HR. However, the experiments in Fig. 8 show that the curl from the front fan becomes serious, showing an opposite tendency.

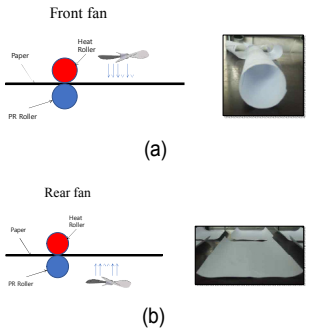


Fig. 8. Analysis of the effect of fan location: (a) The fan at the HR side; (b) the fan at the PR side.

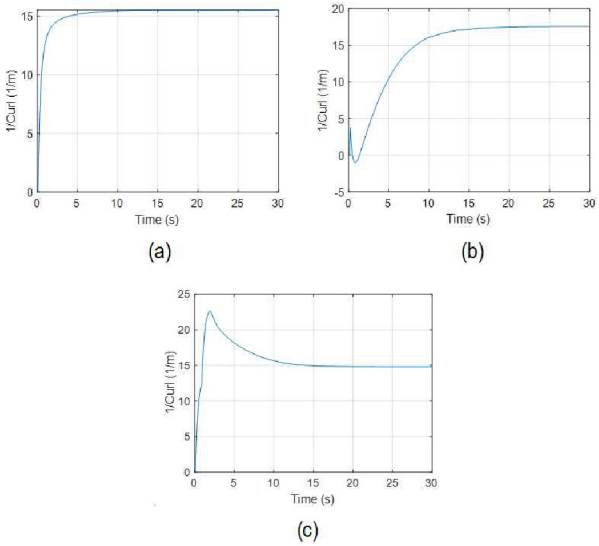


Fig. 9. Simulation results of the fan model: (a) Curl evolution without fan (curvature = 15.5427 $m^{-1}$); (b) curl evolution with the fan at the HR side (curvature = 17.5605 $m^{-1}$); (c) curl evolution with the fan at the PR side (curvature = 14.7802 $m^{-1}$).

We introduce a scaling factor for the fan effect on the convection coefficients of moisture and temperature to present the fan model.

$$K_m = \begin{cases} K_m & \text{Fan turn off} \\ K_m + \alpha_{fan} & \text{Fan turn on} \end{cases}$$

$$\alpha_{fan} = \begin{cases} 0 & \text{Before fan } (0\ \text{s} \le t < 1\ \text{s}) \\ K_{air} & \text{Under fan } (1\ \text{s} \le t \le 2\ \text{s}) \\ K_{air}\psi & \text{After fan } (2\ \text{s} < t) \end{cases} \quad (16)$$

$$K_h^{air} = \begin{cases} K_h^{air} & \text{Fan turn off} \\ K_h^{air} + \alpha_{fan}^h & \text{Fan turn on} \end{cases}$$

$$\alpha_{fan}^h = \begin{cases} 0 & \text{Before fan } (0\ \text{s} \le t < 1\ \text{s}) \\ K_{air}^h & \text{Under fan } (1\ \text{s} \le t \le 2\ \text{s}) \\ K_{air}^h\psi & \text{After fan } (2\ \text{s} < t) \end{cases} \quad (17)$$

where $\psi$ is the scaling factor. In the simulation, $\psi$ is set to 0.4 and convection coefficients $K_{air}$ and $K_h^{air}$ are set to 0.011 $ms^{-1}$ and 11.48 $Wm^{-2}K^{-1}$, respectively. We assume that the paper sheet passes under the blowing zone of the fan between 1 and 2 s. The related coefficients are modified because the blow from the fan affects the convection of temperature and moisture between the paper sheet and air. Therefore, the thermal and mass convection coefficients are increased by two times when the paper sheet is directly under the fan blowing zone and by 1.4 times after the paper sheet passes through the blowing zone. The paper sheet is assumed to be indirectly affected by the blown air at $t$ = 2 s.

Fig. 9 shows the simulation results of the fan model. The simulation shows that the curl toward the HR is generated because the fan is placed at the HR side, as expected in the beginning. However, the evaporation from the bottom surface increases the inverse curl, as shown in Fig. 9(b).

With the fan at the PR side, the paper losing moisture caused by evaporation absorbs large amount of moisture from air after passing the fan. Therefore, the curl decreases.

## 4. Conclusions

In this study, we proposed a multiphysics model including the moisture transport, heat transfer, and mechanical deformation to predict the paper curl passing through the fuser nip in laser printers. The moisture exchange and transport in the fiber and pore matrices caused by the change in temperatures were considered in the integrated model. The contraction and extension of the paper sheet caused by moisture transport were described using a viscoplastic model. The curvature of the paper sheet was effectively calculated using a two-spring model. The proposed model provided an in-depth understanding of the curling mechanisms. The temperature differences on the surfaces causes the moisture gradient along the thickness of the paper. Stresses are developed because of the constraints of the rollers inside the nip, and curls are generated toward the low-temperature side because of the escape of more moisture. The calculated curls at various temperatures agree well with the experimental measurements. The simulation results show that the paper curls significantly increase with the increases in the temperature of the HR and the temperature difference between the HR and PR. The temperature- and moisture-dependent paper properties will be studied and quantitatively compared with the experimental measurements in future work. The multiphysics model will be expanded by including the path curl occurring after the fuser nip, and the integrated model will be used to calculate the entire curl generated during printing. The simulation results will provide useful data for the engineering design of printers. The proposed model can be used for other engineering problems related to moisture and temperature transport inside materials, such as moisture-related deformation problems in airplane composites and building structures, and controlling the shape of micro/nano-structures using moisture.

## Acknowledgments

This work was supported by the research grant of HP, the National Research Foundation of Korea grant of the Korean government Ministry of Science and ICT (no. 2018R1A5A 7025522), and the research program of Dongguk University, 2020.

## References

[1] S. Lee and G. H. Yoon, Moisture transport in paper passing through the fuser nip of a laser printer, *Cellulose*, 24 (8) (2017) 3489-3501.

[2] A. H. Bedane, H. Xiao and M. Eić, Water vapor adsorption equilibria and mass transport in unmodified and modified cellulose fiber-based materials, *Adsorption*, 20 (7) (2014) 863-874.

[3] A. Bandyopadhyay, B. Ramarao and S. Ramaswamy, Transient moisture diffusion through paperboard materials, *Colloids Surf A*, 206 (1) (2002) 455-467.

[4] A. Bandyopadhyay, H. Radhakrishnan, B. V. Ramarao and S. G. Chatterjee, Moisture sorption response of paper subjected to ramp humid changes: Modeling and experiments, *Industrial & Engineering Chemistry Research*, 39 (1) (2000) 219-226.

[5] A. E. Saez, C. J. Otero and I. Rusinek, The effective homogeneous behavior of heterogeneous porous media, *Transport in Porous Media*, 4 (3) (1989) 213-238.

[6] M. Lindner, Factors affecting the hygroexpansion of paper, *Journal of Materials Science*, 53 (1) (2018) 1-26.

[7] M. Alava and K. Niskanen, *The physics of paper, Reports on Progress in Physics*, 69 (3) (2006) 669-723.

[8] P. Lipponen, T. Leppänen, J. Kouko and J. Hämäläinen, Elasto-plastic approach for paper cockling phenomenon: On the importance of moisture gradient, *International Journal of Solids and Structures*, 45 (11) (2008) 3596-3609.

[9] M. L. Dano and J. P. Bourque, Deformation behavior of paper and board subjected to moisture diffusion, *International Journal of Solids and Structures*, 46 (6) (2009) 1305-1316.

[10] T. Mohammadnejad and A. R. Khoei, An extended finite element method for hydraulic fracture propagation in deformable porous media with the cohesive crack model, *Finite Elements in Analysis and Design*, 73 (2013) 77-95.

[11] D. Soares and L. C. Wrobel, Solution of hyperbolic bioheat conduction models based on adaptive time integrators, *Finite Elements in Analysis and Design*, 149 (2018) 1-14.

[12] P. A. Larsson and L. Wågberg, Diffusion-induced dimensional changes in papers and fibrillar films: Influence of hydrophobicity and fibre-wall cross-linking, *Cellulose*, 17 (5) (2010) 891-901.

[13] P. A. M. Zapata, M. Fransen, J. ten Thije Boonkkamp and L. Saes, Coupled heat and moisture transport in paper with application to a warm print surface, *Applied Mathematical Modeling*, 37 (12) (2013) 7273-7286.

[14] J. Fan and X. Wen, Modeling heat and moisture transfer through fibrous insulation with phrase change and mobile condensates, *International Journal of Heat and Mass Transfer*, 45 (19) (2002) 4045-4055.

[15] A. H. Bedane, M. Eić, M. Farmahini-Farahani and H. Xiao, Theoretical modeling of water vapor transport in cellulose-based materials, *Cellulose*, 23 (3) (2016) 1537-1552.
[16] H. Gupta and S. G. Chatterjee, Parallel diffusion of moisture in paper. Part 1: Steady-state conditions, *Industrial and Engineering Chemistry Research*, 42 (25) (2003) 6582-6592.
[17] H. Gupta and S. G. Chatterjee, Parallel diffusion of moisture in paper. Part 2: Transient conditions, *Industrial and Engineering Chemistry Research*, 42 (25) (2003) 6582-6592.
[18] P. Harrison, M. F. Alvares and D. Anderson, Towards comprehensive characterization and modeling of the forming and wrinkling mechanics of engineering fabrics, *International Journal of Solids and Structures*, 154 (2018) 2-18.
[19] E. Bosco, R. H. J. Peerlings, B. A. G. Lomans, C. G. van der Sman and M. G. D. Geers, On the role of moisture in triggering out-of-plane displacement in paper: From the network level to the macroscopic scale, *International Journal of solids and Structures*, 154 (2018) 66-77.
[20] M. E. Parker, J. E. Bronlund and A. J. Mawson, Moisture sorption isotherms for paper and paperboard in food chain conditions, *Packaging Technology and Science: An International Journal*, 19 (4) (2006) 193-209.
[21] E. J. Quirijins, A. J. Van Boxtel, W. K. van Loon and G. Van Straten, Sorption isotherms, GAB parameters and isosteric heat of sorption, *Journal of the Science of Food and Agriculture*, 85 (11) (2005) 1805-1814.
[22] W. Ramberg and W. R. Osgood, *Technical Note No. 902 Description of Stress-strain Curves by Three Parameters*, National Advisory Committee for Aeronautics, Washington DC (1943).
[23] H. Huang, C. Ye and V. Sun, Moisture transport in fibrous clothing assemblies, *Journal of Engineering Mathematics*, 61 (1) (2008) 35-54.

**Gil Ho Yoon** received his B.S., M.S., and Ph.D. degrees in Mechanical and Aerospace Engineering from Seoul National University in 1998, 2000, and 2004, respectively. He currently serves as a Professor at the School of Mechanical Engineering in Hanyang University, Seoul, Republic of Korea.

**Taehan Kim** leads the mechanical simulation team of HP Printing Korea (formerly Printing Solution Business at Samsung Electronics). He has worked at the automotive and printing industry for more than 20 years. His current research interests include modeling and analyzing the multidisciplinary area of printing system, including multiphysics simulation. He received his Ph.D. in aeronautics and astronautics with specialization in composite structures from Stanford University.

**Byoungho Yoo** received his B.S. and M.S. degrees in naval ocean engineering from Seoul National University in 1996. He has worked on mechanical computer-aided engineering, including vibration and paper path dynamics, at Samsung Electronics Printing Division and at HP since 2017.

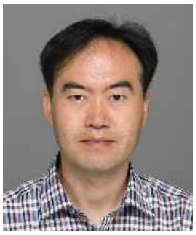

**Woon Kyung Kim** is a Senior Research Engineer of the mechanical simulation team at HP Printing Korea, Pangyo, Korea. He received his Ph.D. degree in mechanical engineering from Virginia Tech, Virginia, USA, with specialization on smart material systems and structures. His research interests include multifunctional composite structure analysis, dynamic simulation, and optimization design of laser printing systems.

**Junseong Woo** is a Senior Research Engineer of the CAE team at HP Printing Korea, Pangyo, Korea. He received his M.S. degree in mechanical engineering from Ajou University, Korea, with specialization on structural fatigue of multi-body systems. His research interests include paper behavior and dynamic simulation of printer units for improving image defects.

**Seungjun Lee** is an Assistant Professor of Mechanical, Robotics, and Energy Engineering at Dongguk University, Seoul, Korea. He received his B.S. degree in naval architecture and ocean engineering from Seoul National University and his M.S. and Ph.D. degrees in mechanical engineering from the University of Michigan, Ann Arbor, Michigan, USA. His research interest includes multi-scale simulations and mechanical behavior at nano/microscales.